**This is the Pre-Published Version.**
This is the Accepted Manuscript version of an article accepted for publication in 2D Materials. IOP Publishing Ltd is not responsible for any errors or omissions in this version of the manuscript or any version derived from it. The Version of Record is available online at https://doi.org/10.1088/2053-1583/aa55b2.
This manuscript version is made available under the CC-BY-NC-ND 4.0 license (https://creativecommons.org/licenses/by-nc-nd/4.0/).

# *In-situ* observation of the thermal stability of black phosphorus

*Shenghuang Lin[1,2,4], Yanyong Li[1,4], Wei Lu[1,4], Ying San Chui[1], Lukas Rogée[1], Qiaoliang Bao[2,3] and Shu Ping Lau[1]*

1. Department of Applied Physics, The Hong Kong Polytechnic University, Hung Hom, Kowloon, Hong Kong (China)

2. Institute of Functional Nano and Soft Materials (FUNSOM), Jiangsu Key Laboratory for Carbon-Based Functional Materials and Devices, and Collaborative Innovation Center of Suzhou Nano Science and Technology, Soochow University, Suzhou 215123, P. R. China

3. Department of Materials Science and Engineering, Monash University, Clayton, VIC 3800, Australia

4. S. H. Lin Y. Y. Li and W. Lu contributed equally to this work

E-mail: *apsplau@polyu.edu.hk*

Keywords: black phosphorus, solution-processable, phase-transition, in-situ

Supplementary material for this article is available online

**Abstract**

Two-dimensional (2D) layered black phosphorus (BP), with a direct band gap and high carrier mobility, has shown great potential for next generation electronics and optoelectronics. However, 2D materials always show different thermal properties when compared to its bulk counterpart. Therefore, it is necessary to understand the thermal process of BP to reveal its natural physical properties. Herein, an atomic-scale microscopic and spectroscopic study is performed to characterize the thermal degradation and re-deposition of solution-exfoliated BP. The *in-situ* decomposition temperature of the BP is observed to be greater than 400 °C. The residual gaseous BP would be re-deposited to form amorphous phosphorus when the chamber was cooled down to room temperature. Moreover, the thickness of the BP flakes can be moderately controlled through thermal thinning process. Our study provides an insight into the thermal stability of 2D BP in vacuum and opens an avenue in fabricating large-area ultra-thin BP films.

## Introduction

Two-dimensional (2D) van der Waals crystals, a type of atomically thin materials without dangling bonds on their surface, have attracted much attention around the world and revealed good potential in electronic devices due to their unique physical, chemical and mechanical properties [1-16]. To deeply understand the fundamental properties of such materials beyond bulk state, several methods have been proposed and developed to fabricate them at atomic scale. Generally, there are two basic categories for synthesizing 2D materials, including top-down and bottom-up methods [17]. Top-down methods prepare 2D nanostructures by isolating one or few atomic layers from the bulk via external energy (mechanical/ultrasonic energy). In contrast, the bottom-up methods can form 2D nanostructures by depositing the atoms on a substrate through thermal and/or chemical reactions. Typically, exfoliation and chemical vapor deposition (CVD) are the most commonly used methods for preparing 2D nanostructures. Particularly CVD method can synthesize large-area and device-grade 2D materials uniformly [18-21]. However, to the best of our knowledge, layered black phosphorus (BP) films cannot be synthesized by CVD. The main reason may be the harsh conditions of preparing bulk BP, which needs high temperature and ultrahigh pressure when using red phosphorus as source [22]. It means layered BP may be grown by CVD at high temperature and high pressure. Therefore, it is necessary to investigate the thermal decomposition of BP at different temperatures, hence to provide insight for preparing BP film.

The melting point of bulk BP varies from 600 °C to >1000 °C [23-26], the exact melting point of BP is still in debate. Thus, it is of significance to investigate the thermal stability parameters of layered BP. Recently, Liu *et al.* reported the decomposition of BP occurred at ~400 °C in vacuum [27], which is the first *in-situ* TEM investigation of thermal behavior of layered BP under vacuum and electron beam irradiation. However, the investigated BP flake was exposed under electron beam for a long time and the BP could be damaged because of the high energy electron irradiation. Meanwhile, the detailed thermal decomposition process of BP flakes in vacuum is still lacking. Herein, we quantitatively observe the thermal decomposition and re-deposition process of the solution-exfoliated BP by *in-situ* TEM, followed by energy-dispersive X-ray spectroscopy (EDX). The morphological and

spectroscopic measurements reveal that the *in-situ* sublimation temperature of the solution-exfoliated BP is greater than 400 °C. It revealed that the BP flakes would be decomposed gradually when heated up in vacuum and the gaseous BP would be re-deposited to form amorphous P when the chamber was cooled down. According to our investigation, we proposed a thermal annealing method to gradually etch the BP.

**Results and discussion**

The ultrathin BP flakes were exfoliated from bulk BP in iso-propyl alcohol (IPA) solution by an ultrasonication method [28]. The thickness distribution of the as-obtained BP flakes is shown in Figure S1. It can be found that the thickness of the BP flakes is ranging from 2 to 22 nm. The BP solution was drop-casted onto silicon nitride grid embedded in a heating E-chip and loaded into the TEM chamber for measurement. The schematic diagram of an E-chip is shown in Figure S2. Here two BP flakes were selected for *in-situ* TEM observation and to be heated at the same time. Figure 1a shows a bright field TEM image for an exfoliated BP flake, revealing its orthorhombic crystalline character confirmed by the selected area electron diffraction (SAED) pattern as shown in the inset of Figure 1b. Figure 1b reveals the lattice fringes of the BP by high-resolution TEM (HRTEM). It can be seen the lattice spacing of the BP flake is ~0.21 nm, which corresponds to (0 0 2) crystal plane according to ICDD-PDF: No.76-1963. The energy-dispersive X-ray spectroscopy (EDX) spectrum in the inset implies the entire selected flake is pure phosphorous. Figure 1c-f show the morphology of the BP flake at different heating stages with the insets providing the corresponding SAED patterns. The heating time for each stage was kept for 5 mins with a heating rate of 10 °C /min. Meanwhile the electron beam was shifted to blank area to reduce the irradiation time on the BP flake. Compared with the case of the BP flake at 350 °C stage (Figure 1f), the wrinkles (marked by red dash arrows) becomes obvious and then disappears as the temperature rises up. A circle round halo of SAED pattern shown in the inset of Figure 1f indicates the flake becomes amorphous after 350 °C annealing for 5 min. It should be noted that the BP flake was exposed to the electron beam for 1 to 3 min in order to preform SAED and HRTEM, which induces the degradation of the BP flake when performed imaging. Therefore, the effect of the electron beam irradiation on the sample should be taken into consideration before

determining the phase-transition temperature of the BP flake.

In order to investigate the irradiation damage from the electron beam of the TEM, we further study another BP flake at a starting temperature of 350 °C as shown in Figure 2a. The inset shows the SAED pattern from the BP, revealing the high crystalline quality of the BP. When the temperature is increased to 400 °C and then 450 °C (Figure 2b and 2c), the BP flake still reveals good crystalline quality according to the SAED patterns as shown in the inset of Figure 2b and 2d. By comparing Figure 2a with Figure 2b, we can find that the studied area in Figure 2b looks brighter than that at 350 °C while the tilting angle and beam intensity remain unchanged. It means that the thickness contrast of the BP at 350 °C is higher than that at 400 °C, suggesting part of the BP is decomposed. As the temperature increases, the BP flake is decomposed gradually as shown in Figure 2c. The insets in Figure 2a, b and d show the HRTEM images of the BP flake at 350 °C, 400 °C and 450 °C, respectively, revealing the BP flake with high crystalline quality. The crystal plane spacing of the sample is ~0.21 nm, which corresponds to (0 0 2) crystal plane of orthorhombic phosphorus by ICDD-PDF: No.76-1963. It is subtle to note that the crystal phase of the studied BP flake changes from monocrystalline to amorphous but the flake's morphology remains when the sample is kept at a temperature of 450 °C for 5 min while the electron beam is shifted (see Figure 2e & 2f). It should be noted here that it takes several minutes for increasing the temperature and maintaining at 450 °C before the BP flake is exposed to the electron beam. In short, the TEM electron-beam radiation time will influence the observed melting temperature of the BP flake.

In addition, we also investigate the thermal decomposition process of the BP at a temperature of 450 °C. Figure 3 shows the HRTEM images of the *in-situ* observation of the thermal decomposition process at different stages of the BP flake. At the initial stage with t = 0 s, the top layer of the BP flake is nearly completely covering the whole surface. The obvious boundary (as shown in Figure 3a marked by yellow dash arrow) can be seen between the top and bottom parts of the BP flake. The bottom and top parts of the BP flake are indicated by the red and black ovals respectively. As the experiment proceeds on, the boundary shifts from left to right as shown in Figure 3b-3h (from stage t = 4s to stage t = 51s), until the top part of the flake disappears (Figure 3h). The lattice of the top layer shifts from left to right side on the studied BP flake. The real-time thermal decomposition process can be found in the supporting

video. In other words, it implies the thickness of the BP flake can be easily controlled through thermal decomposition. Figure S3 illustrate the possible thermal deposition mechanism. At the initial stage, the top layer is completely stacked with the bottom layer. As heating proceeds, the top layer will be gradually decomposed until it vanishes (as the stages I -IV in Figure S3). Then the next layer will be decomposed again when the top layer of the flake completely evaporates (stage V). As the heating continues, the decomposed process will repeat until the whole flake is completely decomposed.

Moreover, we also need to know the re-deposition process of the evaporated gas in a typical CVD or other vacuum system, e.g., BP as a precursor to form blue phosphorus [29]. Herein, we quantitatively observe the re-depositing behavior of phosphorus gas in vacuum. Namely, we monitor the phosphorus content change on the studied sample when decreasing the heating temperature at a rate of 10 °C/min from 450 °C to room temperature. As shown in Figure S4a, the shape of the previously studied BP flake stays the same, and the corresponding SAED pattern (Figure S4b) reveals the BP flake remaining amorphous even cooled down to room temperature. Through quantitatively analyzing the phosphorus content by EDX in Figure S4c and d, we can find the relative weight of the phosphorus element is increased from 3.79% to 5.72% when decreasing the temperature from 100 °C to 25 °C, which implies the phosphorus gas can be redeposited during cooling process in vacuum. However, the re-deposited BP film still exhibit amorphous phase, which may be due to the lack of high pressure for preparing BP [30]. Namely, the phase-transition occurred with a process shown as follow:


Then it can be concluded that there existed one phase-transition for BP, from monocrystalline phase to amorphous phase, when increasing the temperature to 450 °C, but no phase change occurred during the cooling process. In other words, CVD BP film cannot be obtained under vacuum conditions without the assistant of an ultra-high pressure of 10 kbar [30]. Therefore, large area BP film can possibly be fabricated by CVD method under ultra-high pressure when using BP crystal as source.

Inspired by the above results, we also performed an experiment to control the thickness of the

BP flakes through thermal annealing. The size of the solution-processable BP flakes is relatively small (~ 100 nm) according to our previous work [28], which cannot be observed using optical microscope. Therefore, we utilized mechanically exfoliated BP flakes to perform the thermal annealing experiment. As shown in Figure 4a and 4b, the BP flakes are firstly exfoliated onto $SiO_2$/Si substrate and then placed into a tube furnace for thermal thinning. The thickness of the as-prepared BP flake is ~65.9 nm as shown in Figure 4c. Figure 4d shows the typical Raman spectrum of the studied BP flake with vibrational modes of $A^1_g$ (362 $cm^{-1}$), $B_{2g}$ (438 $cm^{-1}$) and $A^2_g$ (467 $cm^{-1}$), which are corresponding well to the featured Raman positions of BP [31-34]. To precisely control the thickness of the BP flake by thermal annealing, we set the target heating temperature at 400 °C for thermal annealing. The thickness of the BP flake is reduced from 65.9 nm to 8.3 nm within 7 mins (Figure 4e and Figure S5). The thinning process begins from the edges to the center of the samples as shown in Figure 4e and S5. The experimental and fitting curves can be found in Figure 5a. The thinning rate exhibits a linear dependence on the heating time. The thickness varies with heating time can be nearly expressed as $y_{\text{thickness}}$ (nm) = 66 - 8.6$t$, where $y$ is the thickness of the BP flake, $t$ represents the heating time. It also implies that the Raman peak positions (Figure 5b) of the BP show little shifts when the thickness is thinned down to 8.3 nm, which is in good agreement with Castellanos-Gomez *et al.* [35] but a little different from the simulation [36]. Meanwhile, the Figure 5c also shows the Raman intensity ratio of $A_g^1$/Si decreases exponentially with the increase of heating time, which reveals the studied BP flake became thinner as the heating time increases. It also offers an additional evidence that the BP flake can be thinned down through thermal process.

The device performanc of the BP-based field effect transistor (FET) before and after thermal thinning process was examined. The FET based on the pristine mechanically exfoliated BP flake with the thickness of ~40 nm is defined device D1. After the characterization, the as-prepared device was annealed at 400 °C for 1 min (D2) in a tune furnace. The transport property of the annealed device (D2) was measured. Subsequently, the device was annealed totally for 3 min (D3) and then 4 min (D4) at 400 °C. The typical I-V characteristics of these devices measured at various back gate voltages from -80 to 0 V are shown in Figure S6a, c, e, g. Meanwhile, the devices show the similar gating effect behaviors. Namely, the output

current is increased by increasing gate voltages before and after the thermal thinning, which implies the p-type semiconductor behavior of both pristine and annealed BP flakes. Figure S6b, d, f, h show the output current of the devices, applied with a varied $V_{DS}$ of 10 - 40 mV, are measured as a function of $V_G$. The field-effect mobility was extracted from the linear region by $\mu=g_mL/C_GV_{DS}W$, where $g_m = dI_{DS}/dV_G$, $C_G$ is the gate capacitance, and $L$ (10 μm) and $W$ (5 μm) are the length and width of the device channel, respectively. The average hole mobility can be up to ~179, 617, 207 and 358 $cm^2V^{-1}S^{-1}$ for D1, D2, D3 and D4, respectively. The corresponding on/off ratio for D1, D2, D3 and D4 is extracted to be 1.19, 3.45, 1.86 and 1.91 respectively. The reason why we got such low on/off ratio may be due to the thicker BP covered by the gold electrodes. In this study, the real thinning area is the channel between the electrodes exclude the parts below the contacts because the gold electrodes can serve as a protective layer to prevent the evaporation of BP at some extent. In addition, we know the thermal annealing plays a key role in the device performance of the BP and other 2D materials [37-39]. The field-effect mobility of the BP can be as high as ~1,350 $cm^2V^{-1}s^{-1}$ at room temperature after annealing at 300 - 500°C [37]. Therefore, the increase of hole mobility for BP from 179 (D1) to 617 $cm^2V^{-1}S^{-1}$ (D2) can be attributed to the contact effect. As for the D2 and D3, the reason for the decrease of mobility may be due to both the thermal annealing and thinning process. After the flakes are thinned further for D3 and D4, the effects of thinning process should dominate the devices performance, resulting in the increase of mobility from 207 to 358 $cm^2V^{-1}S^{-1}$.

**Conclusion**

In summary, a suite of atomically precise microscopy and spectroscopy techniques have been employed to characterize the *in-situ* thermal degradation and re-deposition of solution-processable 2D BP. It can be found the *in-situ* sublimation temperature of solution-exfoliated 2D BP is greater than 400 °C. The thermal decomposition process of the BP flakes revealed that the bulk BP can be thinned to atomically thin layer through thermal annealing. The gaseous BP would be re-deposited to form amorphous P when the chamber was cooled down to room temperature. Our study quantitatively provides insight into the thermal stability of the 2D BP and opens an avenue in fabricating large-area ultra-thin BP

films.

**Experimental Section**

*Preparation of BP flakes for in-situ observation*: BP crystal was purchased from Smart Elements. About 5 mg of BP crystals was added into 4 mL of iso-propyl alcohol (IPA) solution grounded in a mortar. Then the BP crystal was firstly ground for 10 min to form small size BP powder. After that, the mixture was poured into a glass bottle (with a volume of 4 mL) to be ultrasonicated using an ultrasonic bath of 400 W at a temperature of 28 °C for 24 hrs. The obtained BP solution was centrifugaed with rates of 4000 rpm for 30 min in order to remove larger particles.

*Characterizations of BP flakes*: Raman spectra were collected using a Horiba Jobin Yvon HR800 Raman microscopic system equipped with a 488 nm laser operating at 180 mW. The spot size of the excitation laser is ~1 μm. The AFM measurements were performed in a Veeco Dimension-Icon system with a scanning rate of 0.972 Hz. The *in-situ* observation was conducted on a JEM-2100F scanning transmission electron microscope (STEM) equipped with energy dispersive X-ray (EDX) operated at 200 kV and a Protochips Aduro™ platform with a heating E-chip specimen support (the amorphous SiN film was pre-coated on the E-chip) which is capable of providing ultra-high stability, low drift at high temperature, and accurate temperature control. The details can be found in the supporting information.

*Thermal thinning of exfoliated BP flakes*: Mechanically exfoliated BP flakes were firstly transferred from the bulk BP onto $SiO_2$/Si substrate, and then placed into a one-inch diameter tube furnace for thermal annealing. The distance between the center and BP sample is ~10 cm (the length of the heating zone in the CVD furnace is ~20 cm). The temperature and vacuum level for thermal heating is ~400 °C and ~4 Pa respectively.

*Fabrication and Characterization of BP FET*: BP flake was firstly transferred onto $SiO_2$/Si substrate. Electrodes were then patterned by electron beam lithography and Ti/Au (5 nm/60 nm) was evaporated for contact electrodes. Electrical measurements were performed at room temperature in ambient conditions using a probe station equipped with semiconductor property analyzers (Keithley 4200).

**Acknowledgements**

S.H. Lin, Y.Y. Li and W. Lu contributed equally. This work was financially supported by PolyU grants (Project no. 1-ZE14 and 1-ZVGH). One of the authors (SHL) acknowledges the support from the Postdoctoral Science Foundation of China (No. 7131701013), Hong Kong Scholars Program (No. G-YZ36) and the postdoctoral early development program of Soochow University (No. 32317156 & No. 32317267). Q. Bao acknowledges the support from 863 Program (Grant No. 2013AA031903), the youth 973 program (2015CB932700), and the NSFC grants (Grant No. 51222208, 51290273, 91433107).

**References**

[1] Novoselov K S, Fal'ko V I, Colombo L, Gellert P R, Schwab M G and Kim K 2012 A roadmap for graphene *Nature* 490 192-200

[2] Wang Q H, Kalantar Zadeh K, Kis A, Coleman J N and Strano M S 2012 Electronics and optoelectronics of two-dimensional transition metal dichalcogenides *Nat. Nanotechnol.* 7 699-712

[3] Geim A K and Grigorieva I V 2013 Van der Waals heterostructures *Nature* 499 419-25

[4] Mak K F, Lee C, Hone J, Shan J and Heinz T F 2010 Atomically Thin $MoS_2$: A New Direct-Gap Semiconductor *Phys. Rev. Lett.* 105 136805

[5] Splendiani A, Sun L, Zhang Y, Li T, Kim J, Chim C Y, Galli G and Wang F 2010 Emerging Photoluminescence in Monolayer $MoS_2$ *Nano Lett.* 10 1271-1275

[6] Feng J, Qian X f, Huang C W and Li J 2012 Strain-engineered artificial atom as a broad-spectrum solar energy funnel *Nat. Photonics.* 6 866-872

[7] Radisavljevic B, Radenovic A, Brivio J, Giacometti V and Kis A 2011 Single-layer MoS2 transistors *Nat. Nanotechnol.* 6 147-50

[8] Bernardi M, Palummo M and Grossman J C 2013 Extraordinary sunlight absorption and one nanometer thick photovoltaics using two-dimensional monolayer materials *Nano Lett.* 13 3664-70

[9] Kim S, Konar A, Hwang W S, Lee J H, Lee J, Yang J, Jung C, Kim H, Yoo J B, Choi J Y, Jin Y W, Lee S Y, Jena D, Choi W and Kim K 2012 High-mobility and low-power thin-film transistors based on multilayer MoS2 crystals *Nat. Commun.* 3 1011

[10] Frey G L, Reynolds K J, Friend R H, Cohen H and Feldman Y 2003 Solution processed anodes from layer structure materials for high efficiency polymer light emitting diodes *J. Am. Chem. Soc.* 125 5998-6007

[11] Yin Z, Li H, Li H, Jiang L, Shi Y, Sun Y, Lu G, Zhang Q, Che X and Zhang H 2012 Single layer MoS2 phototransistors *ACS Nano* 6 74-80

[12] Yoon Y, Ganapathi K and Salahuddin S 2011 How good can monolayer $MoS_2$ transistors be? *Nano Lett.* 11 3768-73

[13] Geim A K 2009 Graphene: Status and Prospects *Science* 324 1530

[14] Schwierz F 2010 Graphene transistors *Nat. Nanotechnol.* 5 487-96

[15] Dery H, Wu H, Ciftcioglu B, Huang M, Song Y, Kawakami R, Shi J, Krivorotov I, Zutic I and Sham L J 2012 Nanospintronics Based on Magnetologic Gates *IEEE Trans. Electron Devices* 59 259-262

[16] Geim A K and Novoselov K S 2007 The rise of graphene *Nature Mater.* 6 183-191

[17] Das S, Sudhagar P, Kang Y S and Choi W 2014 Graphene synthesis and application for solar cells *J. Mater. Res.* 29 299-319

[18] Li X, Cai W, An J, Kim S, Nah J, Yang D, Piner R, Velamakanni A, Jung I, Tutuc E,

Banerjee S K, Colombo L and Ruoff R S 2009 Large-Area Synthesis of High-Quality and Uniform Graphene Films on Copper Foils *Science* 324 1312

[19] Zhan Y, Liu Z, Najmaei S, Ajayan P M and Lou J 2012 Large-area vapor-phase growth and characterization of $MoS_2$ atomic layers on a $SiO_2$ substrate *Small* 8 966-71

[20] Kang K, Xie S, Huang L, Han Y, Huang P Y, Mak K F, Kim C J, Muller D and Park J 2015 High-mobility three-atom-thick semiconducting films with wafer-scale homogeneity *Nature* 520 656-60

[21] Xu Z Q, Zhang Y, Lin S, Zheng C, Zhong Y L, Xia X, Li Z, Sophia P J, Fuhrer M S, Cheng Y B and Bao Q L 2015 Synthesis and Transfer of Large-Area Monolayer WS2 Crystals: Moving Toward the Recyclable Use of Sapphire Substrates *ACS Nano* 9 6178-6187

[22] Park C M and Sohn H J 2007 Black Phosphorus and its Composite for Lithium Rechargeable Batteries *Adv. Mater.* 19 2465-2468

[23] Akahama Y, Utsumi W, Endo S, Kikegawa T, Iwasaki H, Shimomura O, Yagi T and Akimoto S 1987 Melting curve of black phosphorous *Phys. Lett. A* 122 129-131

[24] Brazhkin V V and Zerr A J 1992 Relative stability of red and black phosphorus at P<1 GPa *J. Mater. Sci.* 27 2677-2681

[25] Kikegawa T, Iwasaki H, Fujimura T, Endo S, Akahama Y, Akai T, Shimomura O, Yagi T, Akimoto S and Shirotani I 1987 Synchrotron-radiation study of phase transitions in phosphorus at high pressures and temperatures *J. Appl. Crystallogr.* 20 406-410

[26] Madelung O, *Semiconductors: Data Handbook*. Springer Berlin Heidelberg: **2012**;

[27] Liu X, Wood J D, Chen K S, Cho E and Hersam M C 2015 In Situ Thermal Decomposition of Exfoliated Two-Dimensional Black Phosphorus *J. Phys. Chem. Lett.* 6

773-778

[28] Lin S, Liu S, Yang Z, Li Y, Ng T W, Xu Z, Bao Q, Hao J, Lee C S, Surya C, Yan F and Lau S P 2016 Solution-Processable Ultrathin Black Phosphorus as an Effective Electron Transport Layer in Organic Photovoltaics *Adv. Func. Mater.* 26 864-871

[29] Zhang J L, Zhao S T, Han C, Wang Z Z, Zhong S, Sun S, Guo R, Zhou X, Gu C D, Yuan K D, Li Z Y and Chen W 2016 Epitaxial Growth of Single Layer Blue Phosphorus: A New Phase of Two-Dimensional Phosphorus *Nano Lett.* 16 4903–4908.

[30] Li L, Yu Y, Ye G J, Ge Q, Ou X, Wu H, Feng D, Chen X H and Zhang Y 2014 Black Phosphorus Field-Effect Transistors *Nat. Nanotechnol.* 9 372-377

[31] Liu H, Neal A T, Zhu Z, Luo Z, Xu X, Tománek D and Ye P D 2014 Phosphorene: An Unexplored 2D Semiconductor with a High Hole Mobility *ACS Nano* 8 4033-4041

[32] Koenig S P, Doganov R A, Schmidt H, Castro Neto A H and Özyilmaz B 2014 Electric field effect in ultrathin black phosphorus *Appl. Phys. Lett.* 104 103106

[33] Buscema M, Groenendijk D J, Blanter S I, Steele G A, van der Zant H S and Castellanos Gomez A 2014 Fast and broadband photoresponse of few-layer black phosphorus field-effect transistors *Nano Lett.* 14 3347-52

[34] Li Y Y, Hu Z X, Lin S H, Lai S K, Ji W and Lau S P 2016 Giant Anisotropic Raman Response of Encapsulated Ultrathin Black Phosphorus by Uniaxial Strain *Adv. Func. Mater.* ***(DOI:*** *10.1002/adfm.201600986)*

[35] Andres C G, Leonardo V, Elsa P, Joshua O I, Acharya K L N, Sofya I B, Dirk J G, Michele B, Gary A S, Alvarez J V, Henny W Z, Palacios J J and Herre S J v d Z 2014 Isolation and characterization of few-layer black phosphorus *2D Mater.* 1 025001

[36] Cai Y, Ke Q, Zhang G, Feng Y P, Shenoy V B and Zhang Y W 2015 Giant Phononic Anisotropy and Unusual Anharmonicity of Phosphorene: Interlayer Coupling and Strain Engineering *Adv. Func. Mater.* 25 2230-2236

[37] Chen X, Wu Y, Wu Z, Han Y, Xu S, Wang L, Ye W, Han T, He Y, Cai Y and Wang N 2015 High-quality sandwiched black phosphorus heterostructure and its quantum oscillations *Nat. Commun.* 6 7315

[38] Namgung S D, Yang S, Park K, Cho A-J, Kim H and Kwon J-Y 2015 Influence of post-annealing on the off current of MoS2 field-effect transistors *Nanoscale Res. Lett.* 10 1-6

[39] Hui Y Y, Tai G a, Sun Z, Xu Z, Wang N, Yan F and Lau S P 2012 n- and p-Type modulation of ZnO nanomesh coated graphene field effect transistors *Nanoscale* 4 3118-3122

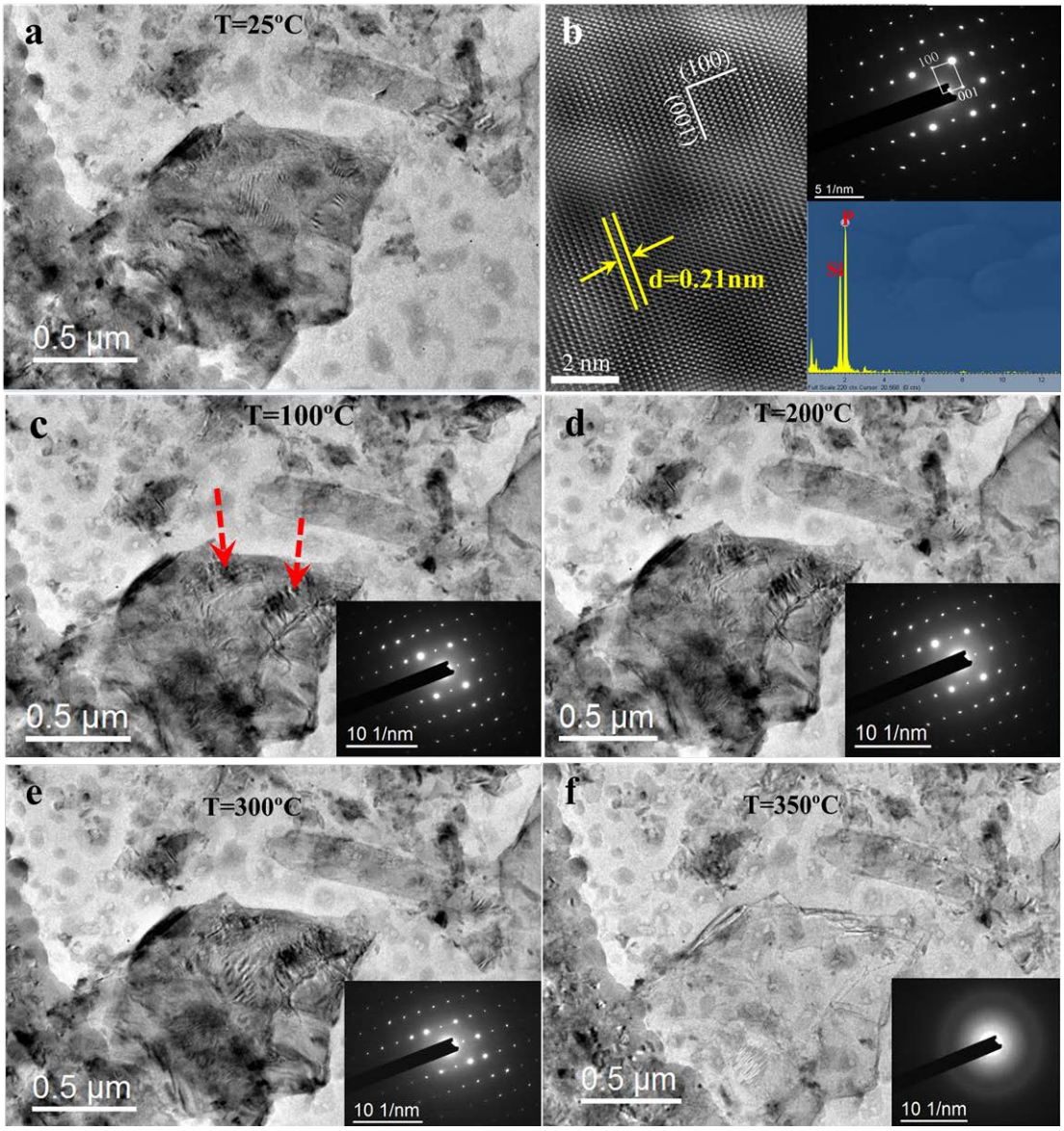


**Figure 1**. TEM images of the BP flake and *in-situ* heating of BP. **(a)** Low-magnification TEM bright field image of a BP flake at room temperature. **(b)** The Fast Fourier transformation of high-resolution TEM image of the BP showing lattice fringes. The crystal plane spacing is ~0.21 nm, corresponding to (0 0 2) crystal plane according to ICDD-PDF: No.76-1963. Insets: Selected area electron diffraction (SAED) pattern and EDX spectrum of the flake. (c-f) TEM bright field images of the BP flake after loading into the TEM chamber and heating at **(c)** 100 °C, **(d)** 200 °C, **(e)** 300 °C, **(f)** 350 °C, respectively. All heating times are 5 min. Insets: SAED patterns for each heating stage. From the SAED patterns, amorphization occurs at 350 °C. The red dash arrows show the wrinkles areas on the BP surface.

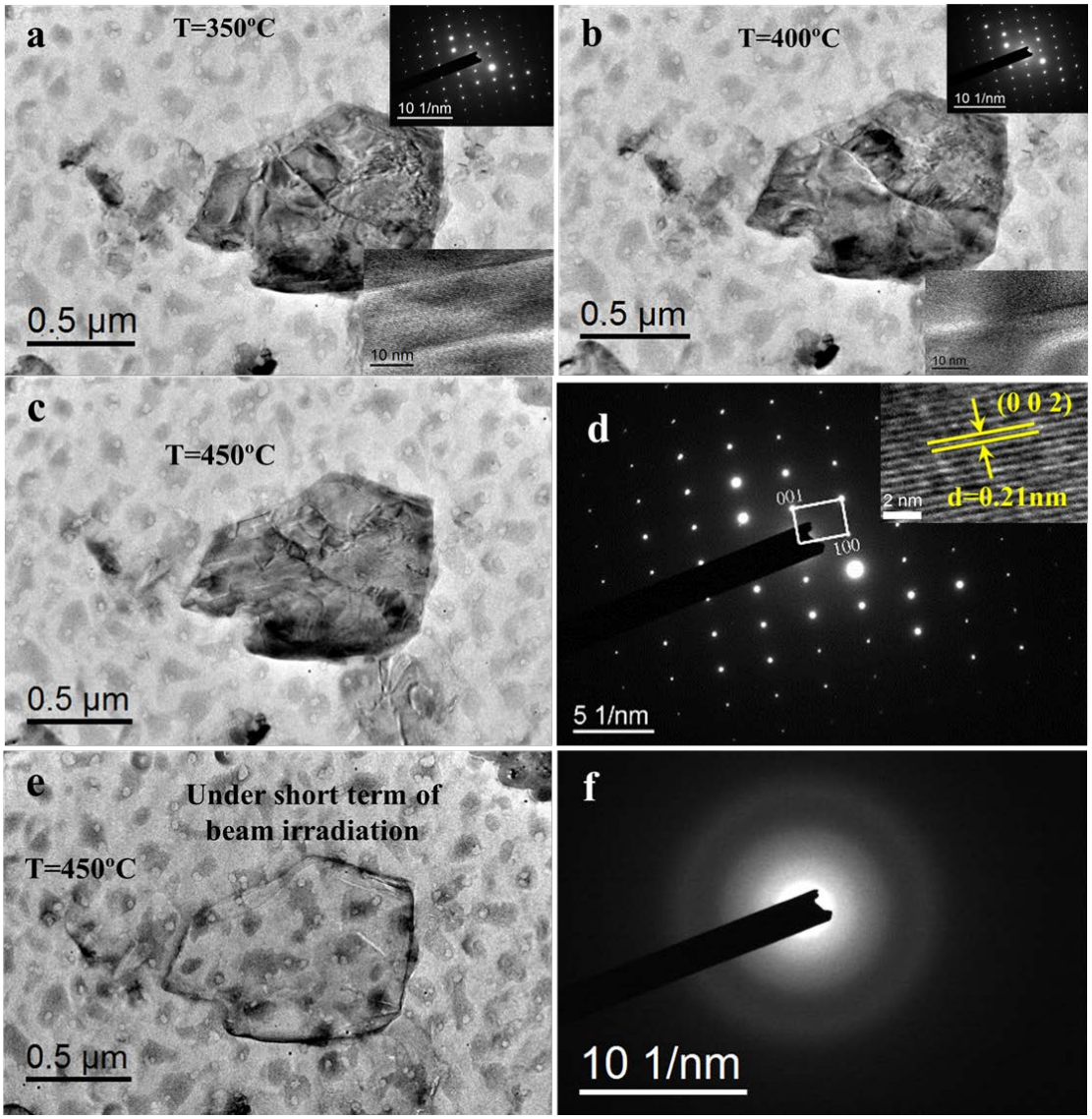


**Figure 2**. TEM images of another BP flake by *in-situ* heating. **(a-c)** Low-magnification TEM bright field image of the BP flake, without electron beam radiation before, heating at 350 °C, 400 °C and 450 °C respectively. Insets in **(a)** and **(b)** denote the corresponding SAED pattern. SAED and high resolution TEM image of the BP in **(d)** showing its high-crystalline quality and lattice fringes. The crystal plane spacing is ~0.21 nm, corresponding to (0 0 2) crystal plane according to ICDD-PDF: No.76-1966. **(e)** The BP flake was kept at 450 °C for a longer time without beam irradiation, which reveals the wrinkles disappears, as well as the BP flake becomes amorphous as shown in (f). Namely, the phase-transition of the BP crystal from single crystal to amorphous will happen at 450 °C with short term of beam irradiation during this process.

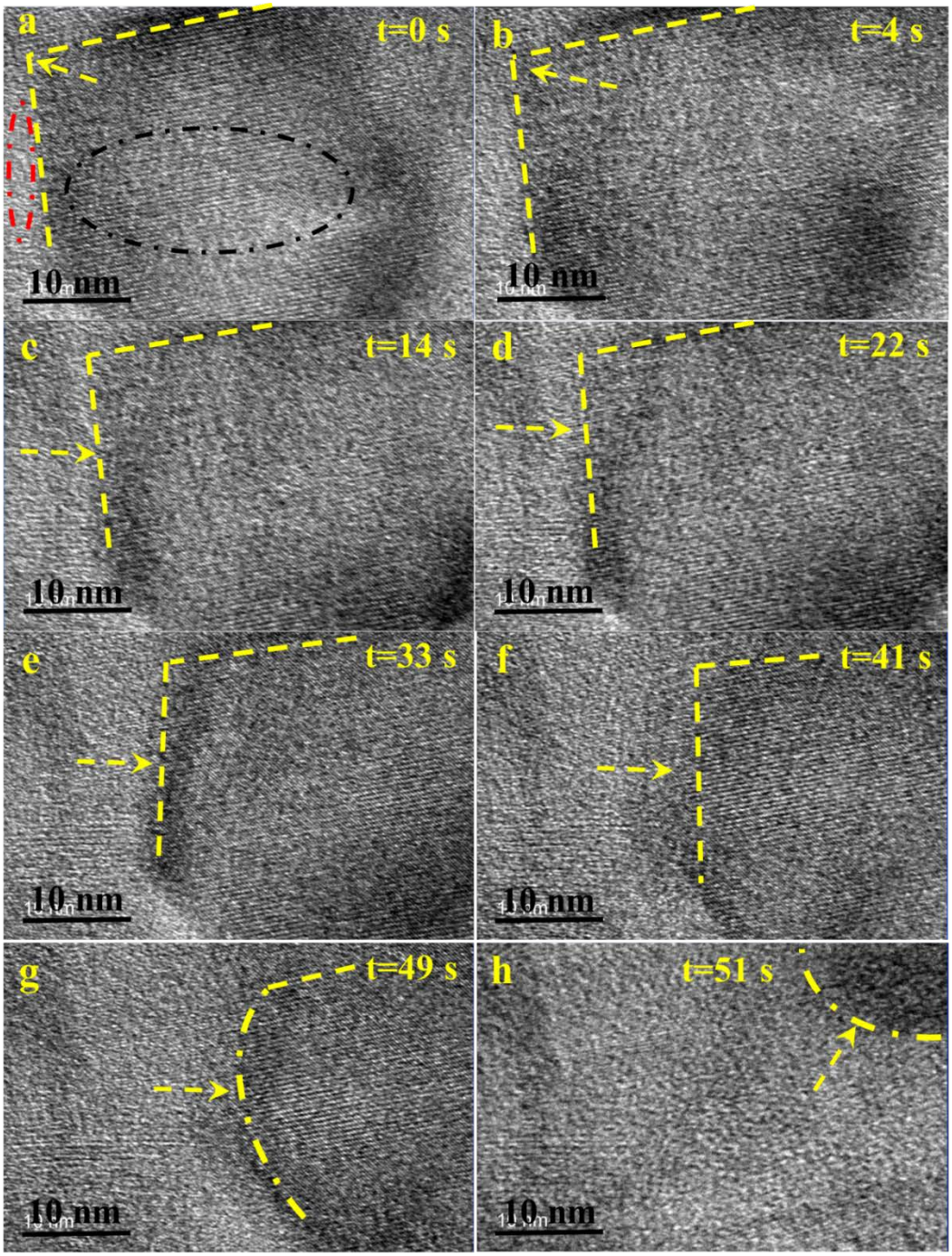


**Figure 3**. HRTEM images of *in-situ* observation of the thermal decomposition of the BP flake at different stages: **(a)** Initial stage at t = 0 s; **(b)** t = 4 s; **(c)** t = 14 s; **(d)** t = 22 s; **(e)** t = 33 s; **(f)** t = 41 s; **(g)** t = 49 s; **(h)** t = 51 s. The bottom and top layers of the BP are marked by red and black ovals, respectively. The yellow arrow represents the boundary between the top and bottom part BP. All the images are taken at 450 °C. It can be seen that, as the experiment proceeds on, the boundary between top and bottom BP shifts from left to right, revealing the top part of the BP finally disappearing.

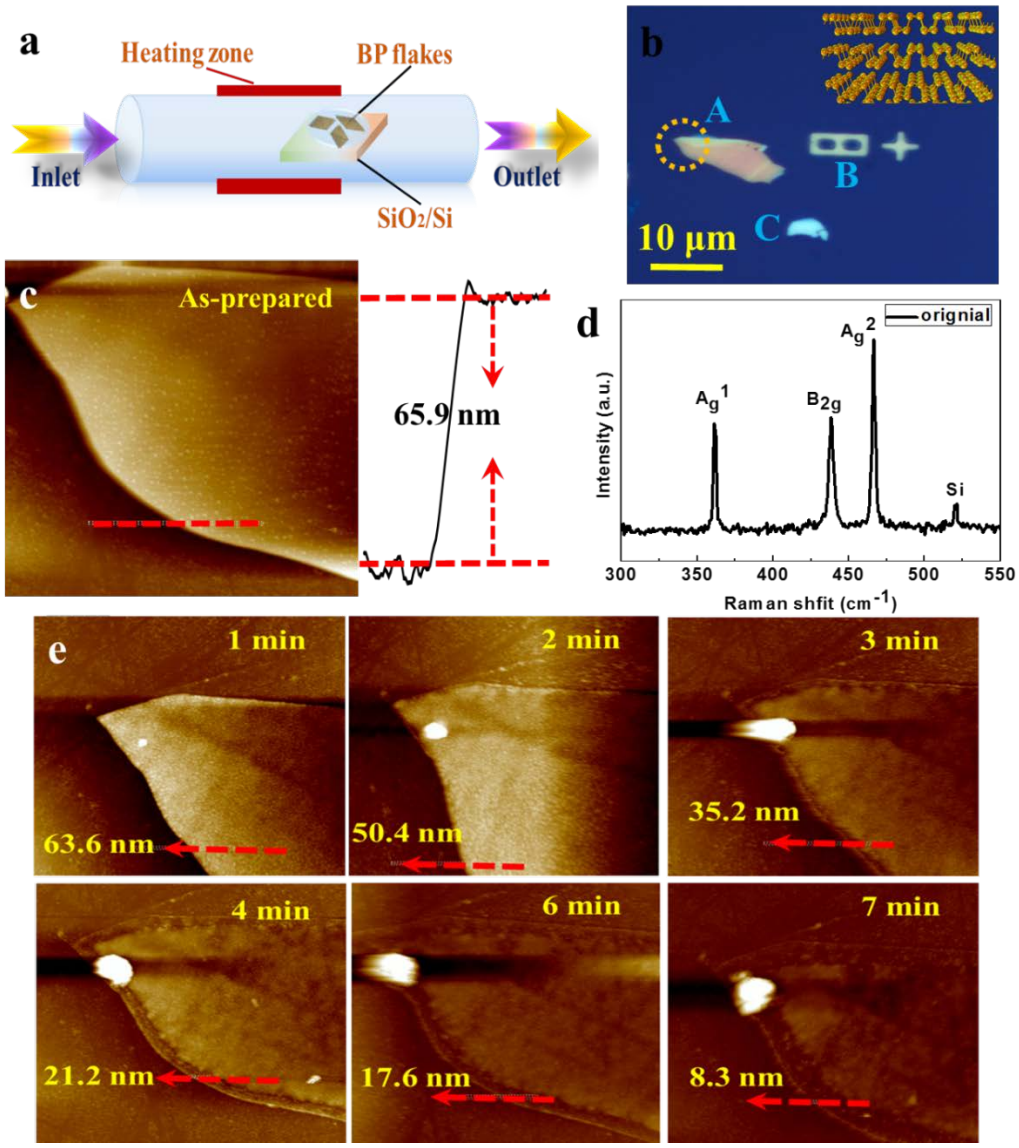


**Figure 4. (a)** Schematic illustration of the mechanically exfoliated BP flakes placed into tube furnace for thermal annealing. The samples were kept at ~10 cm away from the center of the furnace. **(b)** Optical image of the BP flakes transferred onto $SiO_2$/Si substrate. The inset shows the schematic crystal structure of the BP. Point A and C represent BP flakes, B reveals the mark on the substrate. The yellow dash circle marked the studied area on the BP flake by AFM. **(c)** AFM image of the as-prepared BP flake. It reveals the thickness of the measured area as marked by red dash line is ~65.9 nm. **(d)** The Raman shift of the three BP modes measured at the red dash line marked in (c). **(e)** AFM images of the mechanically exfoliated BP flakes after thermal thinning at 400°C. It can be seen the thickness of the BP flake is obviously reduced, revealing the successful thinning process. Red arrows implied the measured region of the BP.

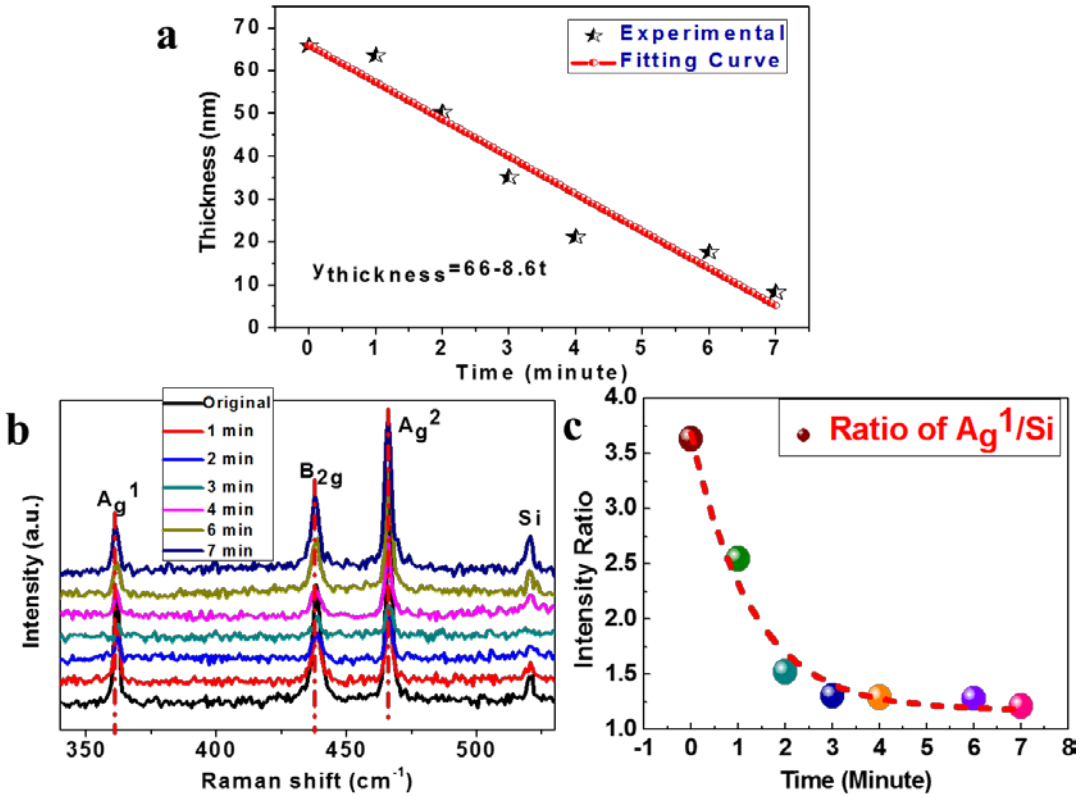


**Figure 5**. **(a)** Experimental and fitting curves of BP thickness varies with the heating time. **(b)** Raman spectra of the BP flake at different heating stages. It reveals the feature Raman peaks of $A^1_g$, $B_{2g}$ and $A^2_g$ have no big changes with the annealing time. **(c)** It reveals the Raman intensity ratio of $A_g^1$/Si as the heating time goes.